$NaNO_3$ monolayer: A stable graphenelike supersalt with strong four-phonon scattering and low lattice thermal conductivity insensitive to temperature

Tingwei Li (李廷炜),[1] Peng-Hu Du (杜鹏虎),[1] Ling Bai (白羚),[1] Qiang Sun (孙强),[1,2,*] and Puru Jena[3]

[1]*School of Materials Science and Engineering, Peking University, Beijing 100871, China*

[2]*Center for Applied Physics and Technology, Peking University, Beijing 100871, China*

[3]*Department of Physics, Virginia Commonwealth University, Richmond, Virginia 23284, USA*

(Received 23 March 2022; revised 23 May 2022; accepted 31 May 2022; published 21 June 2022)

Since the discovery of graphene, numerous efforts have been made to seek new two-dimensional (2D) graphenelike materials with intriguing properties. Here,we report a stable graphenelike supersalt $NaNO_3$ monolayer composed of superhalogen NO_3. The 2D $NaNO_3$ monolayer is found to possess an ultralow isotropic Young's modulus (2.983 N/m) and a low thermal conductivity (1.65 W/mK @300 K), which is much lower than that of 2D NaCl monolayer (3.72 W/mK @300 K). We attribute this behavior to the strong anharmonicity induced by the weak bonding between Na and NO_3 cluster and the large atomic displacements of O in the NO_3 cluster. A giant four-phonon scattering leads to a 60% reduction in lattice thermal conductivity at 300 K compared to that of three-phonon scattering. Furthermore, temperature-induced phonon hardening causes the lattice thermal conductivity to be nearly temperature independent in the studied temperature range (100–350 K), displaying significant difference from the atom-based 2D materials.

DOI: 10.1103/PhysRevMaterials.6.064009

I. INTRODUCTION

Graphene is a 2D material consisting of a single layer of carbon atoms arranged in a honeycomb lattice. Motivated by its remarkable properties and technological applications in optoelectronics, transistors, thermal management, and energy storage devices [1–5], many other graphenelike 2D materials have been predicted and synthesized [6–8]. In contrast to the planar honeycomb configuration, the silicene, germanene, and stanene, predicted by theory [9,10] and synthesized by experiments [11–13], have buckled honeycomb lattice. Furthermore, the 2D materials of group IIIA (borophene [14], Gallenene [15]), group VA (phosphorene, arsenene, antimonene, and bismuthene) [16] as well as group VIA (selenene and tellurene) [17] have also been found to have the buckled honeycomb structure. Besides above monoelemental 2D materials, 2D honeycomb compounds such as *h*-BN [18], IIA-VIA (BeO, MgO, CaO, ZnO, CdO, CaS, SrS, SrSe, BaTe, and HgTe) [19] and IVA-VIA XY (X = C, Si, Ge, Sn; Y = O, S, Se, Te) [20], and BSi monolayers [21] have gained tremendous interest.

Recently, new graphenelike monolayer composed of monochlorides (NaCl, LiCl, and AgCl) have been predicted by first-principles calculations [22]. The monolayer sodium chloride (NaCl) is of special interest because its bulk counterpart is the common table salt. The negative binding energy of the 2D NaCl monolayer implies that this exotic hexagonal structure could be experimentally synthesized, which has been confirmed by Kseniya *et al.* [23] through the growth of the hexagonal NaCl thin films on the (110) diamond substrate. It has been demonstrated that replacing halogens by superhalogens (i.e., clusters with electron affinities larger than that of Cl, namely, 3.61 eV) could lead to a new class of materials with unprecedented properties because of their unique size, symmetry, and electronic structure [24–26]. Note that NO_3, with an electron affinity of 3.937 ± 0.014 eV [27] is a superhalogen cluster anion and is a building block of a variety of compounds, such as three-dimensional nitrate salts $LiNO_3$, KNO_3, $Mg(NO_3)_2$, $Ca(NO_3)_2$, hypersalt molecules $KLi(NO_3)_2$, $KMg(NO_3)_3$, and $KAl(NO_3)_4$ [28], and ionic liquid (BMIM-NO_3) [29]. However, there is no report of NO_3 as a building block of 2D graphenelike crystal, which motivated this study. In this paper, we show that not only 2D graphenelike $NaNO_3$ supersalt is stable but its properties are very different from that of 2D-NaCl. We first constructed a graphenelike supersalt 2D $NaNO_3$ monolayer by replacing Cl atoms with NO_3 superatoms in the 2D hexagonal NaCl [Fig. 1(a)] lattice and then systemically investigated its structural, electronic, mechanical, and thermal properties.

II. COMPUTATIONAL METHODS

The energy and electronic structure calculations are performed using the Vienna *Ab initio* Simulation Package (VASP) [30,31]. The interactions between the electrons and ions are described by using projector augmented-wave method [32], which treats the N $2s^2 2p^3$, O $2s^2 2p^4$, Na $2p^6 3s^1$ as valance states. The exchange-correlation functional is treated within the generalized gradient approximation (GGA) [33] using the Perdew-Burke-Ernzerhof (PBE) form [34]. A vacuum layer of 20 Å in the c direction is used to avoid mirror interactions. All atomic positions and cell shape are fully optimized without any symmetry constraint with an energy cutoff of 600 eV and a Gamma-centered k mesh of $9 \times 9 \times 1$. The

*sunqiang@pku.edu.cn

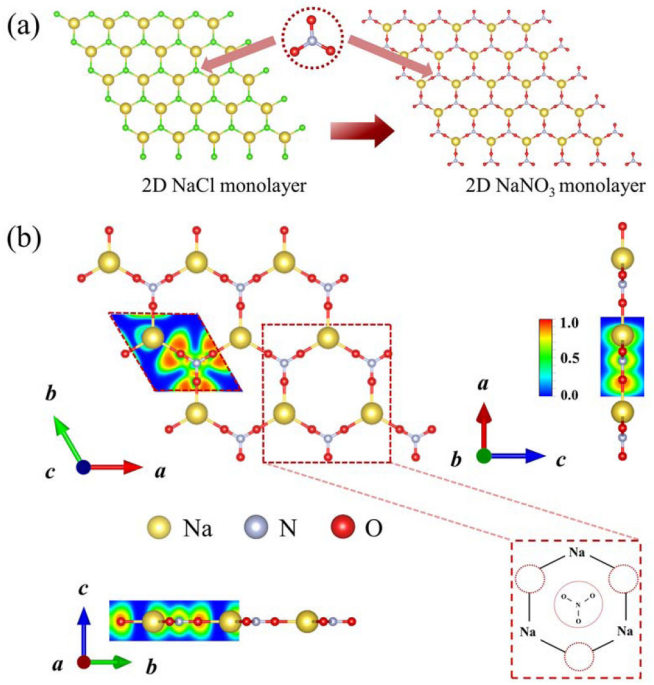

FIG. 1. (a) Schematic diagram of Cl atoms in the 2D NaCl monolayer replaced by NO_3 clusters. The gold, green, gray, and red spheres represent Na, Cl, N, and O atoms, respectively. (b) Geometry and electron localization function of the 2D $NaNO_3$ monolayer. Primitive cell and hexagonal lattice composed of Na atom and NO_3 cluster are plotted in the rhombus and rectangle with red dotted lines, respectively.

convergence criteria for energy and force are 10^{-8} eV and 10^{-6} eV/Å, respectively. As band gaps of semiconductors are underestimated at the PBE level, we used the Heyd-Scuseria-Ernzerhof (HSE06) hybrid functional [35] to obtain a more accurate band gap. We also calculate the dielectric tensors and Born effective charges using the density-functional perturbation theory [36] to include the long-range interactions.

The harmonic interatomic force constants (IFCs) are estimated using a $4 \times 4 \times 1$ supercell and the finite-displacement method as coded in the PHONOPY package [37]. The anharmonic IFCs are extracted within a $4 \times 4 \times 1$ supercell, as implemented in the machine-learning based HIPHIVE package [38]. In detail, we first generate 90 configurations via a Monte Carlo algorithm with random displacements of 0.02 Å. Then we calculate the Hellmann-Feynman forces of each random configuration with a $3 \times 3 \times 1$ k mesh. Finally, based on the displacements-forces of 90 random configurations, the force constants potential (FCP) model and the anharmonic IFCs are fitted through the least absolute shrinkage and selection operator technique [39]. Here, the high-order IFCs are included up to fourth order and the cutoff distances of 11.99, 6.0, and 4.0 Å for the second-, third-, and fourth-order force constants, respectively, are found to be sufficient for convergence.

From the gained FCP model, the self-consistent phonons (SCP) calculations based on the stochastic self-consistent harmonic approximation algorithm [40] are performed to obtain the temperature-dependent phonon frequency. We set mixing parameter α as 0.1 in the SCP iteration. Based on the FCP model, lattice thermal conductivity (k_l) can be obtained by solving the Boltzmann transport equation using the SHENGBTE code [41] with a q mesh of $36 \times 36 \times 1$. We use the full iterative procedure to calculate the three-phonon scattering rates and lattice thermal conductivity, which needs the temperature-dependent second- and third-order IFCs as inputs. Considering the large anharmonicity of cluster-based supersalt-type monolayer, we further involve the four-phonon scattering rates treated at the relaxation time approximation (RTA) level using the FOURPHONON package [42]. The Born effective charges and dielectric constants are used to correct the long-range electrostatic interactions. Since both 2D $NaNO_3$ and NaCl monolayers are flat without the corresponding 3D structures, we choose the van der Waals diameter of Na atom (4.60 Å) [43] as the thickness to calculate their lattice thermal conductivities.

III. RESULTS AND DISCUSSION

A. Structure and bonding

Figure 1(b) shows the geometry of the 2D $NaNO_3$ monolayer having the hexagonal P-6m2 (No. 187) space group. Its primitive cell consists of one Na atom and one NO_3 cluster, featuring a honeycomb lattice with the optimized lattice constant of 5.99 Å. In the NO_3 cluster, one N atom is surrounded by three identically bonded oxygen atoms forming a perfect trigonal planar geometry and all three N–O bond lengths are 1.26 Å. The Na–O bond length has a larger value of 2.19 Å than that of the N–O bond.

To gain insight into the chemical bond characteristics of 2D $NaNO_3$ monolayer, we calculate the electron localization function (ELF) [44]. The values of ELF vary from 0 to 1, where ELF = 1 corresponds to perfect localization and ELF = 0.5 represents delocalized electron gas. The ELF results in Fig. 1(b) show that the electrons are primarily located in the middle between the N and O atoms, exhibiting a strong covalent bond, while for Na atoms and NO_3 clusters, electrons mainly localize around the latter, indicating that ionic bonding dominates the Na–NO_3 bonds. The different length and type of N–O and Na–O bonds result in the hierarchical bond structure in 2D $NaNO_3$ monolayer, which induces special atomic vibrational motions that are responsible for the low thermal conductivity [45]. Furthermore, it has been shown that the number of electrons transferred from Na to NO_3 is 0.91e, which is larger than that of Na to Cl in the 2D NaCl monolayer (0.82e charge) based on the Bader charge analysis. The larger number of electron transfer in the 2D $NaNO_3$ monolayer manifests in the increased bond ionicity, which in turn leads to the asymmetric wave functions and produces anharmonic bonds [46].

B. Energetic, dynamic, and thermal stability

To confirm the stability of the 2D $NaNO_3$ monolayer, we use energetic, dynamic, and thermal stability as three critical factors that need to be satisfied. Here, we choose the formation energy as the energetic stability criteria. The formation energy of the 2D $NaNO_3$ monolayer is defined as $\Delta E_f = E_{NaNO_3} - \frac{1}{2}E_{N_2} - \frac{3}{2}E_{O_2} - E_{Na}$, where E_{NaNO_3} is the total energy of the 2D $NaNO_3$ monolayer, E_{N_2}, E_{O_2}, and E_{Na}

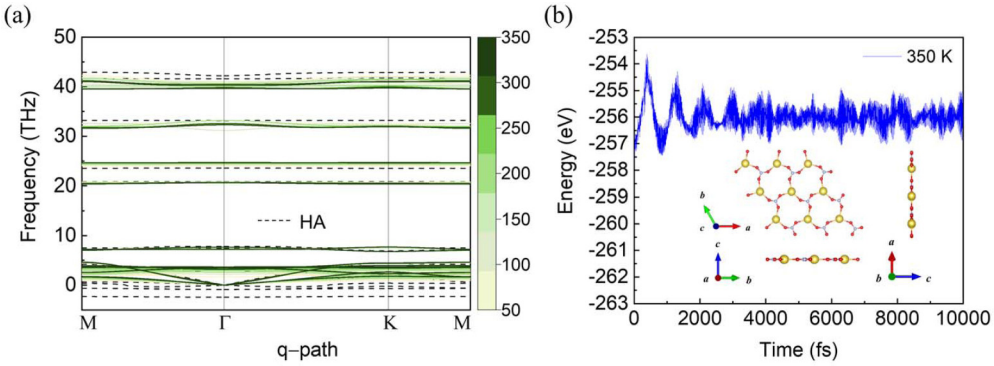

FIG. 2. (a) Phonon dispersions of the 2D $NaNO_3$ monolayer. The solid lines show the results at finite temperatures, and the black dotted lines represent the results for the harmonic approximation (HA). (b) Free-energy changes with respect to time. (Inset) Final structure at 350 K.

are the energies in the most stable phase of Na, N_2, and O_2, respectively. The calculated ΔE_f of the 2D $NaNO_3$ monolayer is -2.875 eV/unit cell, confirming the energetic stability of the 2D $NaNO_3$ monolayer.

The dynamic stability is confirmed by calculating the phonon dispersions; the absence of imaginary frequencies signifies dynamical stability of the material. Figure 2(a) shows the phonon dispersions under harmonic approximation at finite temperatures. The harmonic phonon dispersions show obvious imaginary frequencies. According to the projected phonon density of states (PDOS) of the 2D $NaNO_3$ monolayer, we find that the unstable phonon branches are mainly derived from the O atoms (see Fig. S1 in the Supplemental Material (SM) [47]). The unstable soft modes usually associate with strong lattice anharmonicity [48] or phase transition [49]. To further analyze the vibrations of the unstable phonon branches, we perform a 10 000-step *ab initio* molecular-dynamics simulations (AIMD) at 300 K with 2-fs time step in a $3 \times 3 \times 1$ supercell. The resulting MD trajectories of three random N, O, and Na atoms are plotted in Fig. S2 in the SM [47]. Note that the displacements from the equilibrium position of the O atoms show strong anisotropy. Such large asymmetric displacements of O atoms will enhance the lattice anharmonicity, thus generating the soft modes. Upon including temperature effects, soft modes are all stabilized and continue hardening with increasing temperature. This confirms the dynamic stability of the 2D $NaNO_3$ monolayer at finite temperatures.

Finally, the thermal stability is evaluated by performing an AIMD simulation in a $3 \times 3 \times 1$ supercell. After heating at 350 K for 10 ps with a time step of 2 fs, the total energy is seen to fluctuate around a constant value and the final structure remains intact without bond breaking as depicted in Fig. 2(b). These results prove the energetic, dynamic, and thermal stability of the 2D $NaNO_3$ monolayer.

C. Electronic and mechanical properties

Next we investigate the electronic properties of the 2D $NaNO_3$ monolayer by calculating its band structure and the corresponding total and partial density of states. As seen in Fig. 3(a), the 2D $NaNO_3$ monolayer has a direct band gap of 5.16 eV (3.15 eV) at the Γ point computed using the HSE06 (PBE) functional, which is smaller than that of the 2D NaCl monolayer (6.30 eV at the HSE06 level). From the band-gap values, we can conclude that 2D $NaNO_3$ monolayer is an insulator, which is similar to 2D NaCl monolayer and other 2D alkali halides with the energy band gap ranging from 5.0 to 6.74 eV at the PBE level [50]. The computed partial electron density of states of the 2D $NaNO_3$ monolayer is plotted in Fig. 3(b), which shows that the valence-band maximum (VBM) is mainly determined by the O-p orbitals, and the conduction-band minimum (CBM) is mainly determined by the O-p and N-p orbitals. Specifically, the VBM is contributed by O-p_x and O-p_y orbitals, and the CBM is mainly contributed by O-p_z orbital and N-p_z orbitals. These agree well with the information observed in the band-decomposed charge-density distributions (see Fig. S3 in the SM [47]).

The mechanical properties of the 2D $NaNO_3$ monolayer are explored by calculating in-plane Poisson's ratio $v(\theta)$ and Young's modulus $Y(\theta)$ based on the elastic constants. There are 21 independent elastic constants forming a 6×6 symmetric tensor in a 2D crystal. For this 2D $NaNO_3$ monolayer with hexagonal symmetry, only C_{11} and C_{12} are nonzero and independent. Considering the lattice symmetry above, Poisson's ratio $v(\theta)$ and Young's modulus $Y(\theta)$ as a function of in-plane θ can be expressed as follows [51]:

$$v(\theta) = \frac{C_{12}(\sin^4\theta + \cos^4\theta) - B\sin^2\theta\cos^2\theta}{C_{11}(\sin^4\theta + \cos^4\theta) + A\sin^2\theta\cos^2\theta}, \quad (1)$$

$$Y(\theta) = \frac{C_{11}^2 - C_{12}^2}{C_{11}(\sin^4\theta + \cos^4\theta) + A\sin^2\theta\cos^2\theta}, \quad (2)$$

where $A = 2(C_{11}^2 - C_{12}^2)/(C_{11} - C_{12}) - 2C_{12}$, and $B = 2C_{11} - 2(C_{11}^2 - C_{12}^2)/(C_{11} - C_{12})$. These results are shown in Fig. 4. Poisson's ratio $v(\theta)$ is isotropic with a large value of 0.902 along all directions. This implies that the large elastic deformation against the same strain is equal along different directions. Young's modulus measures the resistance of a material to elastic deformation. In general, a material with low Young's modulus is flexible and elastic. Young's modulus $Y(\theta)$ is found to be isotropic with a value of 2.983 N/m, which is less than those of previously reported 2D materials, such as 1000 N/m for graphene [52] and 330 N/m for MoS_2 [53]. This shows the softness of the 2D $NaNO_3$ monolayer. For comparison, the calculated v and Y of the 2D NaCl monolayer and other 2D monochlorides [50] are given in Table I, showing that the Y of the 2D $NaNO_3$ monolayer is lower than those of

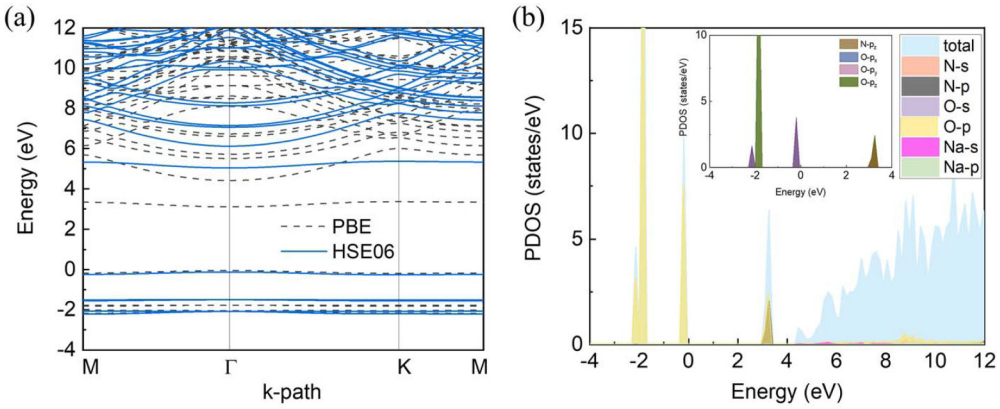

FIG. 3. (a) Electronic band structure and (b) PDOS of the 2D $NaNO_3$ monolayer. (Inset) Enlarged PDOS of O and N atom.

most 2D monochlorides, which indicates the weaker bonding between Na atom and NO_3 cluster compared to the interatomic bonding strength in monolayer atomic compounds. This would lead to slow transport of phonons and low lattice thermal conductivity (κ_l) of 2D $NaNO_3$ monolayer.

D. Lattice thermal conductivity

As unique structures usually lead to intriguing thermal properties, it is of great interest to explore the thermal properties of the 2D $NaNO_3$ monolayer. Slack's rules [54,55] prescribe four characteristics for nonmetallic crystals to have high thermal conductivity. The corresponding rules for crystals to have low thermal conductivity can thus be summarized as having (i) large atomic mass, (ii) weak bonding, (iii) complex crystal structure, and (iv) large anharmonicity. Based on these characteristics, we can expect the 2D $NaNO_3$ monolayer to have a lower lattice thermal conductivity than that of the 2D NaCl monolayer.

The calculated values of κ_l of 2D-$NaNO_3$ and NaCl monolayers are given in Fig. 5. To illustrate the effects of four-phonon (4ph) scattering, we calculate κ_l by first considering three-phonon (3ph) scattering (κ_{3ph}) and then including 4ph scattering ($\kappa_{3,\,4ph}$). The key findings concluded from Fig. 5(a) are as follows: (i) Both κ_{3ph} and $\kappa_{3,\,4ph}$ of the 2D $NaNO_3$ monolayer are lower than those of the 2D NaCl monolayer, and much lower than those of hexagonal BN, BP, BAs [56], C_3N [57], and graphene [58] monolayers with similar low average atomic mass. (ii) Further, considering 4ph scattering, κ_l of 2D $NaNO_3$ monolayer is dramatically reduced from 4.13 to 1.65 W/mK at 300 K, leading to a 60% reduction. (iii) κ_{3ph} of 2D $NaNO_3$ monolayer exhibits very weak temperature dependence. The fitted $\kappa_l - T$ relationships are $T^{-0.06}$ and $T^{-0.17}$, respectively, for κ_{3ph} and $\kappa_{3,4ph}$ of 2D $NaNO_3$ monolayer, which are very different from the corresponding result of $T^{-0.62}$ and $T^{-0.74}$ of 2D NaCl monolayer, indicating the weak temperature dependence of κ_l in superatom crystal. This behavior is significantly different from other typical 2D materials such as graphene, phosphorene [59], and tellurene [60], whose κ_l values are fitted with an inverse relationship with temperature ($\kappa_l \sim 1/T$). In addition, we calculate the mean-free path (MFP) corresponding to the cumulative κ_{3ph} and $\kappa_{3,\,4ph}$ of 2D $NaNO_3$ and NaCl monolayers. Figure 5(b) shows that MFP values corresponding to 80% of $\kappa_{3,\,4ph}$ (κ_{3ph}) are about 52 (159) nm in 2D $NaNO_3$ monolayer, which are much lower than 109 (272) nm in 2D NaCl monolayer. These low values of MFP would result in the low $\kappa_{3,\,ph}$ and $\kappa_{3,\,4ph}$ in 2D $NaNO_3$ monolayer.

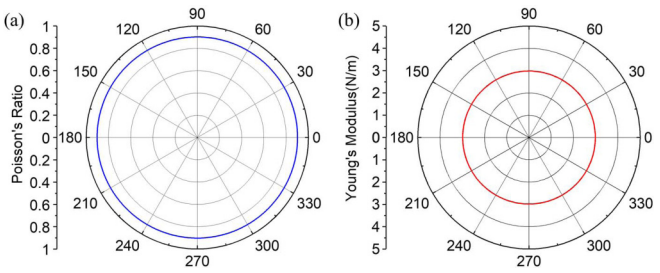

FIG. 4. Polar diagram of (a) Poisson's ratio $\upsilon(\theta)$, and (b) Young's modulus $Y(\theta)$ as a function of the angle θ of the 2D $NaNO_3$ monolayer.

In order to reveal the underlying mechanism for the much lower κ_l of 2D $NaNO_3$ monolayer, we calculate the key factors such as the phonon group velocity (v_q), Grüneisen parameter (γ_λ), 3ph scattering rates (Γ_{3ph}), and 4ph scattering rates (Γ_{4ph}) and compare them with that of NaCl monolayers at 300 K. Because 2D $NaNO_3$ monolayer has smaller average atomic mass than that of 2D NaCl monolayer, the former would have larger values of v_q as shown in Fig. 5(c). The Grüneisen parameter describes the strength of anharmonic interactions of a crystal, which can be defined as $\gamma_\lambda = -\frac{A}{\omega_\lambda}\frac{\partial\lambda}{\partial A}$, where A and ω are the area of the primitive cell and the frequency of a phonon mode λ, respectively. Generally, large $|\gamma|$ implies strong anharmonicity, which accordingly gives rise to low κ_l. As shown in Fig. 5(d), the mode Grüneisen parameters of 2D $NaNO_3$ monolayer cover a wider range, resulting in a larger absolute value of average Grüneisen parameter (4.18) than that of 2D NaCl monolayer (0.71).

The stronger anharmonic interactions contribute to the higher phonon scattering rates of Γ_{3ph} and Γ_{4ph} of 2D $NaNO_3$ monolayer than that of 2D NaCl monolayer at 300 K, as shown in Figs. 5(e) and 5(f). Especially in midlying frequency range (2–5 THz), the bunched optical phonon branches of O atoms restrict the 3ph scattering phase space, but allow 4ph scattering [61]. In contrast, in 2D NaCl monolayer, 4ph

TABLE I. The calculated elastic constants, Poisson's ratio, and Young's modulus of 2D $NaNO_3$, NaCl monolayers, and other 2D monochlorides.

	C_{11} (N/m)	C_{12} (N/m)	Poisson's ratio	Young's modulus (N/m)
2D $NaNO_3$	15.961	14.393	0.902	2.983
2D NaCl	13.602	10.575	0.777	5.379
2D LiCl [50]	18.729	21.398	0.669	10.342
2D KCl [50]	9.844	8.042	0.818	3.268
2D RbCl [50]	8.803	7.209	0.820	2.889

scattering rates are generally smaller than 3ph scattering rates. The giant values of Γ_{4ph} in 2D $NaNO_3$ monolayer reinforce the importance of the quartic anharmonicity on the phonon scattering rates. To further understand the origin of the large anharmonicity, we calculate the atomic displacement parameter (ADPs) of the N and O atoms in NO_3 cluster and Cl atom

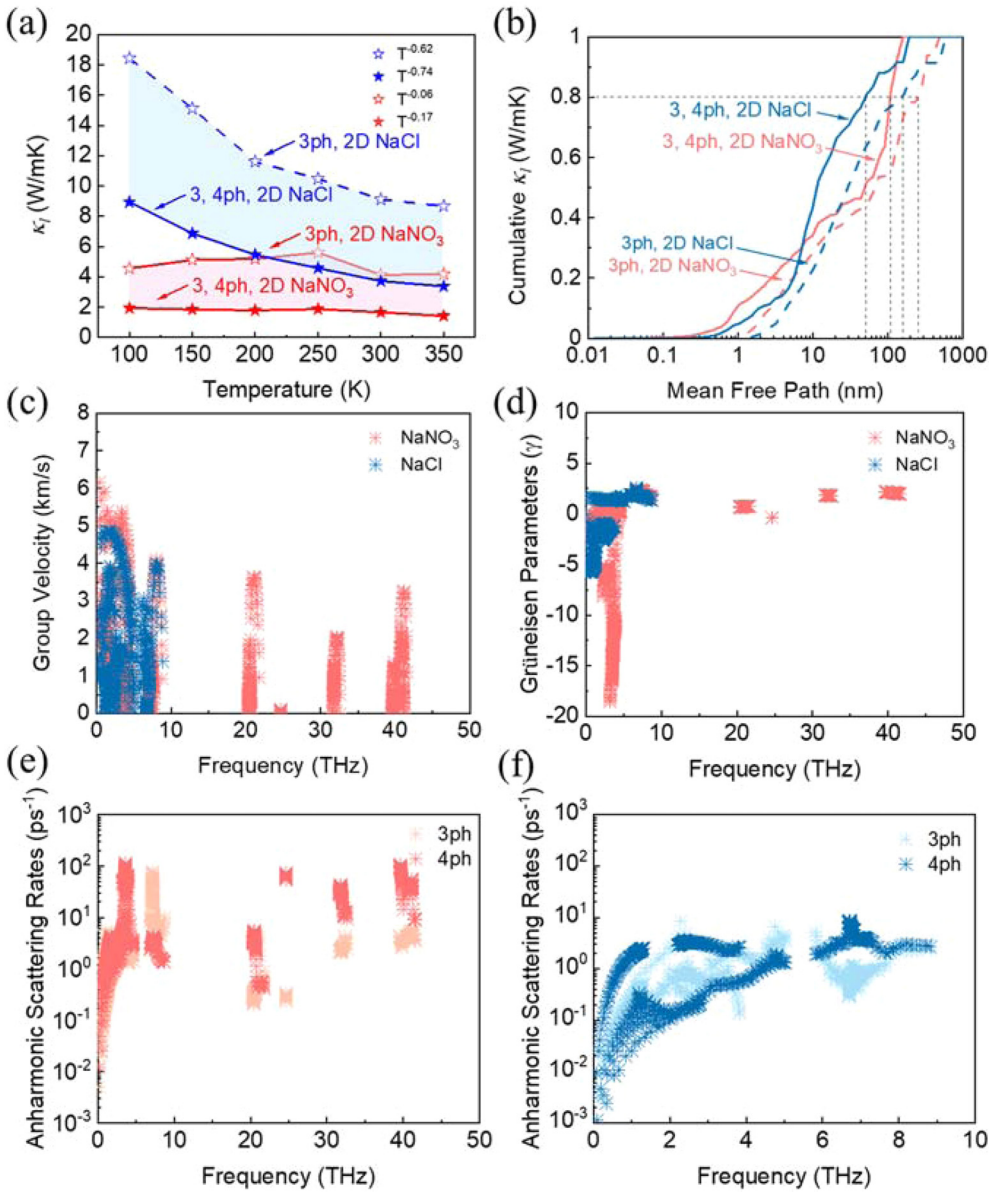

FIG. 5. (a) Changes of κ_l with temperature for 2D $NaNO_3$ and 2D NaCl monolayers. The empty stars denote the values obtained considering only three-phonon (3ph) scattering, whereas the filled stars further include four-phonon (4ph) scattering. (b) Comparison of the cumulative κ_l of 2D $NaNO_3$ (red lines) and 2D NaCl monolayers (blue lines) at 300 K. Dashed and solid lines represent the results excluding and including 4ph scattering, respectively. (c) Group velocity; (d) Grüneisen parameter; and (e), (f) anharmonic scattering rates of 2D $NaNO_3$ and NaCl monolayers at 300 K.

as shown in Fig. S4(a) (see in the SM [47]). The ADPs of the N atom are comparable to that of the Cl atom, but the ADPs of the O atom along the y direction are distinctly larger than those of the Cl atom at all temperatures, which gives rise to the large anharmonicity in the 2D $NaNO_3$ monolayer. Moreover, to clarify the configuration patterns of the O atom clearly, we plot the schematic displacements of O atom in NO_3 cluster based on 300 K AIMD results (see Fig. S4(b) in the SM [47]). The large anisotropic displacements of O atom coupled with these four kinds of displacement modes are as follows: O atoms rotate clockwise or anticlockwise around N atoms, and O atoms move towards or away from N atoms. Multiple configuration modes of O atom in NO_3 cluster enhance the anharmonicity and enlarge 4ph scattering rates in 2D $NaNO_3$ monolayer, thus leading to a low lattice thermal conductivity.

Another remarkable feature of 2D $NaNO_3$ monolayer is its unusual temperature dependence of κ_{3ph}, which can be explained by the effects of phonon hardening on v_q and Γ_{3ph}. An analysis of the frequency-dependent cumulative κ_{3ph} shows that more than 95% of k_{3ph} is contributed by phonon branches in the range of 0–5 THz. In Figs. S5(a) and S5(b) (see in the SM [47]), we plot the v_q and Γ_{3ph} in this frequency range. Note that in the low-lying frequency range associated with acoustic phonon branches (<2 THz), v_q is increased while Γ_{3ph} is surprisingly reduced when temperature increases from 100 to 300 K. These anomalous behaviors are caused by the increased slope of phonon branches and reduced scattering phase induced by the phonon hardening effect (see Fig. S6 in the SM [47]) and thus contribute to the increase of κ_{3ph}. The phonon hardening can be seen more clearly in Fig. S7 in the SM [47], where the total density of states (TDOS) of the 2D $NaNO_3$ monolayer in the frequency range of 0–5 THz shifts toward higher frequency as temperature increases, while in the midlying frequency range, v_q at 300 K is partly lower than those at 100 and 200 K. This can be attributed to bunched phonon branches of O atoms (yellow lines in the SM, Fig. S6) at 300 K. Besides, Γ_{3ph} gets larger with temperature due to the increasing number of phonons, which would hinder phonon transport, thus lowering κ_{3ph}. These two competitive effects lead to an unusual temperature dependence of κ_{3ph}.

IV. CONCLUSION

In conclusion, we propose a honeycomb 2D $NaNO_3$ supersalt monolayer consisting of NO_3 superhalogen as a building block that is energetically, dynamically, and thermally stable. The calculated results show that the 2D $NaNO_3$ monolayer is a direct wide band-gap insulator with a band gap of 5.16 eV and has an ultralow Young's modulus. Especially, strong anharmonicity exists in 2D $NaNO_3$ monolayer, due to the weak bonding between the Na and NO_3 cluster and the large anisotropic ADPs of the O atom in the NO_3 cluster. This makes it necessary to treat anharmonicity up to the quartic term for both phonon scatterings and phonon frequencies. Because of the large 4ph scattering phase space, the strong 4ph scattering significantly reduces the lattice thermal conductivity from 4.13 to 1.65 W/mK in the 2D $NaNO_3$ monolayer at 300 K, which makes it able to be applied in thermal insulation. Unlike other 2D materials reported so far, the lattice thermal conductivity of the 2D supersalt monolayer exhibits very weak temperature dependence. These findings demonstrate the advantages of cluster-based materials over the conventional ones.

ACKNOWLEDGMENTS

This work is partially supported by grants from the National Natural Science Foundation of China (Grant No. NSFC-21973001) and from the Ministry of Science and Technology of China (Grant No. 2021YFB4000601]. P.J. acknowledges partial support by the U.S. Department of Energy, Office of Basic Energy Sciences, Division of Materials Sciences and Engineering under Award No. DE-FG02-96ER45579. Calculations are performed on the High Performance Computing Platform of Peking University, China.

[1] A. K. Geim and K. S. Novoselov, Nat. Mater. **6**, 183 (2007).
[2] A. K. Geim, Science **324**, 1530 (2009).
[3] P. Blake, E. Hill, A. H. Castro Neto, K. Novoselov, D. Jiang, R. Yang, T. Booth, and A. Geim, Appl. Phys. Lett. **91**, 063124 (2007).
[4] A. H. Castro Neto, F. Guinea, N. M. R. Peres, K. S. Novoselov, and A. K. Geim, Rev. Mod. Phys. **81**, 109 (2009).
[5] A. A. Balandin, S. Ghosh, W. Bao, I. Calizo, D. Teweldebrhan, F. Miao, and C. N. Lau, Nano Lett. **8**, 902 (2008).
[6] S. V. Badalov, M. Yagmurcukardes, F. M. Peeters, and H. Sahin, J. Phys. Chem. C. **122**, 28302 (2018).
[7] S. Z. Butler, S. M. Hollen, L. Cao, Y. Cui, J. A. Gupta, H. R. Gutiérrez, T. F. Heinz, S. S. Hong, J. Huang, A. F. Ismach, E. Johnston-Halperin, M. Kuno, V. V. Plashnitsa, R. D. Robinson, R. S. Ruoff, S. Salahuddin, J. Shan, L. Shi, M. G. Spencer, M. Terrones, W. Windl, and J. E. Goldberger, ACS Nano **7**, 2898 (2013).
[8] M. Xu, T. Liang, M. Shi, and H. Chen, Chem. Rev. **113**, 3766 (2013).
[9] K. Takeda and K. Shiraishi, Phys. Rev. B **50**, 14916 (1994).
[10] C.-C. Liu, H. Jiang, and Y. Yao, Phys. Rev. B **84**, 195430 (2011).
[11] P. Vogt, P. De Padova, C. Quaresima, J. Avila, E. Frantzeskakis, M. C. Asensio, A. Resta, B. Ealet, and G. Le Lay, Phys. Rev. Lett. **108**, 155501 (2012).
[12] M. Dávila, L. Xian, S. Cahangirov, A. Rubio, and G. Le Lay, New J. Phys. **16**, 095002 (2014).
[13] F.-f. Zhu, W.-j. Chen, Y. Xu, C.-l. Gao, D.-d. Guan, C.-h. Liu, D. Qian, S.-C. Zhang, and J.-f. Jia, Nat. Mater. **14**, 1020 (2015).
[14] A. J. Mannix, X.-F. Zhou, B. Kiraly, J. D. Wood, D. Alducin, B. D. Myers, X. Liu, B. L. Fisher, U. Santiago, J. R. Guest, M. J. Yacaman, A. Ponce, A. R. Oganov, M. C. Hersam, and N. P. Guisinger, Science **350**, 1513 (2015).

[15] V. Kochat, A. Samanta, Y. Zhang, S. Bhowmick, P. Manimunda, S. Asif S. Asif, A. S. Stender, R. Vajtai, A. K. Singh, C. S. Tiwary, and P. M. Ajayan, Sci. Adv. **4**, e1701373 (2018).

[16] S. Zhang, S. Guo, Z. Chen, Y. Wang, H. Gao, J. Gómez-Herrero, P. Ares, F. Zamora, Z. Zhu, and H. Zeng, Chem. Soc. Rev. **47**, 982 (2018).

[17] L. D. Xian, A. P. Paz, E. Bianco, P. M. Ajayan, and A. Rubio, 2D Mater. **4**, 041003 (2017).

[18] G. Giovannetti, P. A. Khomyakov, G. Brocks, P. J. Kelly, and J. van den Brink, Phys. Rev. B **76**, 073103 (2007).

[19] H. Zheng, X.-B. Li, N.-K. Chen, S.-Y. Xie, W. Q. Tian, Y. Chen, H. Xia, S. B. Zhang, and H.-B. Sun, Phys. Rev. B **92**, 115307 (2015).

[20] C. Kamal, A. Chakrabarti, and M. Ezawa, Phys. Rev. B **93**, 125428 (2016).

[21] L. B. Meng, M. J. Zhou, Y. J. Zhang, and S. Ni, J. Phys.: Condens. Matter **31**, 345401 (2019).

[22] B. Luo, Y. Yao, E. Tian, H. Song, X. Wang, G. Li, K. Xi, B. Li, H. Song, and L. Li, Proc. Natl. Acad. Sci. **116**, 17213 (2019).

[23] K. A. Tikhomirova, C. Tantardini, E. V. Sukhanova, Z. I. Popov, S. A. Evlashin, M. A. Tarkhov, V. L. Zhdanov, A. A. Dudin, A. R. Oganov, D. G. Kvashnin, and A. G. Kvashnin, J. Phys. Chem. Lett. **11**, 3821 (2020).

[24] Y. Gao, M. Wu, and P. Jena, Nat. Commun. **12**, 1331 (2021).

[25] H. Fang and P. Jena, Proc. Natl. Acad. Sci. **114**, 11046 (2017).

[26] T. Li, Q. Sun, and P. Jena, Thermal and thermoelectric properties of cluster-based materials, *Superatoms: Principles, Synthesis and Applications* (Wiley & Sons Ltd, UK, 2021), pp. 317–348.

[27] A. Weaver, D. W. Arnold, S. E. Bradforth, and D. M. Neumark, J. Chem. Phys. **94**, 1740 (1991).

[28] S. Behera, D. Samanta, and P. Jena, J. Phys. Chem. A **117**, 5428 (2013).

[29] A. K. Srivastava, A. Kumar, and N. Misra, J. Phys. Chem. A **125**, 2146 (2021).

[30] G. Kresse and J. Furthmüller, Phys. Rev. B **54**, 11169 (1996).

[31] G. Kresse and J. Furthmüller, Comput. Mater. Sci. **6**, 15 (1996).

[32] P. E. Blöchl, Phys. Rev. B **50**, 17953 (1994).

[33] J. P. Perdew, K. Burke, and M. Ernzerhof, Phys. Rev. Lett. **77**, 3865 (1996).

[34] L. Qiao, S. Zhang, H. Xiao, D. Singh, K. Zhang, Z. Liu, X. Zu, and S. Li, J. Mater. Chem. C **6**, 1239 (2018).

[35] J. Heyd, G. E. Scuseria, and M. Ernzerhof, J. Chem. Phys. **118**, 8207 (2003).

[36] S. Baroni, S. de Gironcoli, A. Dal Corso, and P. Giannozzi, Rev. Mod. Phys. **73**, 515 (2001).

[37] A. Togo and I. Tanaka, Scr. Mater. **108**, 1 (2015).

[38] F. Eriksson, E. Fransson, and P. Erhart, Adv. Theory Simul. **2**, 1800184 (2019).

[39] F. Pedregosa, G. Varoquaux, A. Gramfort, V. Michel, B. Thirion, O. Grisel, M. Blondel, P. Prettenhofer, R. Weiss, V. Dubourg *et al.*, J. Mach. Learn. Res. **12**, 2825 (2011).

[40] I. Errea, M. Calandra, and F. Mauri, Phys. Rev. B **89**, 064302 (2014).

[41] L. Wu, J. Carrete, N. A. Katcho, and N. Mingo, Comput. Phys. Commun. **185**, 1747 (2014).

[42] Z. Han, X. Yang, W. Li, T. Feng, and X. Ruan, Comput. Phys. Commun. **270**, 108179 (2022).

[43] S. S. Batsanov, Inorg. Mater. **37**, 871 (2001).

[44] M. Xu, Y. Q. Cheng, H. W. Sheng, and E. Ma, Phys. Rev. Lett. **103**, 195502 (2009).

[45] J. Yang, Y. Wang, H. Yang, W. Tang, J. Yang, L. Chen, and W. Zhang, J. Phys.: Condens. Matter **31**, 183002 (2019).

[46] J. P. Heremans, Nat. Phys. **11**, 990 (2015).

[47] See Supplemental Material at http://link.aps.org/supplemental/10.1103/PhysRevMaterials.6.064009 for PDOS of the 2D NaNO3 monolayer under harmonic approximation, MD trajectories, band-decomposed charge-density distribution, atomic displacement parameters, phonon group velocity and 3ph anharmonic scattering rates, phonon dispersions, and TDOS.

[48] Y. S. Zhang, E. Skoug, J. Cain, V. Ozolins, D. Morelli, and C. Wolverton, Phys. Rev. B **85**, 054306 (2012).

[49] T. Lanigan-Atkins, S. Yang, J. L. Niedziela, D. Bansal, A. F. May, A. A. Puretzky, J. Y. Y. Lin, D. M. Pajerowski, T. Hong, S. Chi, G. Ehlers, and O. Delaire, Nat. Commun. **11**, 4430 (2020).

[50] P. Kumar, K. Rajput, and D. R. Roy, Mater. Today Commun. **29**, 102855 (2021).

[51] L. Wang, A. Kutana, X. Zou, and B. I. Yakobson, Nanoscale **7**, 9746 (2015).

[52] C. Lee, X. Wei, J. W. Kysar, and J. Hone, Science **32**, 385 (2008).

[53] A. Castellanos-Gomez, M. Poot, and G. A. Steele, Adv. Mater. **24**, 772 (2012).

[54] G. A. Slack, Phys. Rev. **127**, 694 (1962).

[55] G. A. Slack, J. Phys. Chem. Solids **34**, 321 (1973).

[56] H. Fan, H. Wu, L. Lindsay, and Y. Hu, Phys. Rev. B **100**, 085420 (2019).

[57] Y. Hong, J. Zhang, and X. C. Zeng, Nanoscale **10**, 4301 (2018).

[58] B. D. Kong, S. Paul, M. B. Nardelli, and K. W. Kim, Phys. Rev. B **80**, 033406 (2009).

[59] Y. Hong, J. Zhang, X. Huang, and X. C. Zeng, Nanoscale **7**, 18716 (2015).

[60] Z. Shi, R. Cao, K. Khan, A. K. Tareen, X. Liu, W. Liang, Y. Zhang, C. Ma, Z. Guo, X. Luo, and H. Zhang, Nano-Micro Lett. **12**, 99 (2020).

[61] T. Feng, L. Lindsay, and X. Ruan, Phys. Rev. B **96**, 161201(R) (2017).